LOSS OF MeV IONS DURING ^{3}He MINORITY ION CYCLOTRON RESONANCE HEATING IN TFTR

S.J. ZWEBEN, G.W. HAMMETT, R.L. BOIVIN,
C.K. PHILLIPS, J.R. WILSON
Princeton Plasma Physics Laboratory,
Princeton University,
Princeton, New Jersey,
United States of America

ABSTRACT. The loss of D–^{3}He alpha particles to the bottom of TFTR during ^{3}He minority ion cyclotron resonance heating (ICRH) is measured and shown to be consistent with first-orbit loss. However, an anomalous loss also occurs 45° below the outer midplane, which may be due either to a small amount of minority tail ion loss or to ICRH induced deconfinement of fusion products.

1. INTRODUCTION

The fusion reaction D+^{3}He → p (14.6 MeV) + α (3.7 MeV) creates an alpha particle with nearly the same energy as that in the reaction D+T → n (14.1 MeV) + α(3.5 MeV). Therefore, measurements of the confinement and loss of D–^{3}He alpha particles are of interest for planning the upcoming D-T experiments in TFTR, JET and future D–T tokamaks. This paper describes alpha particle loss measurements made during recent ^{3}He ion cyclotron resonance heating (ICRH) experiments on TFTR and presents evidence for an additional ICRH induced MeV ion loss mechanism observed 45° below the outer midplane.

High D–^{3}He fusion reaction rates (comparable to D–D reaction rates) have been obtained in JET [1] and TFTR [2] as a by-product of ^{3}He minority ICRH. Previously, the escaping 14.6 MeV protons were measured in PLT [3–5], PDX [6], TFTR [7] and JET [8], but alpha particle measurements have so far only been made in PLT using a time integrating plastic track detector [9]. Note that the D–^{3}He reaction rate cannot be measured using neutron emission, but it has been measured using the weak gamma emission (from another branch) in JET [10]. Although a fusion gamma diagnostic is being developed in TFTR [11], measurements of D–^{3}He reaction rate data were unavailable for the present experiment.

The escaping MeV ions were measured just outside the limiter radius with the same detectors as used previously for charged D–D fusion products [12], with the detectors 90° and 45° below the outer midplane. The MeV ions enter a pinhole aperture and are dispersed through a slit according to their toroidal pitch angle χ (magnetic moment) in one direction and their gyroradius ρ (energy) in the other. The ions then pass through a 3 μm aluminium foil which blocks low energy ions, and strike a 10 μm thick ZnS(Ag) scintillator screen, the image of which is sent to an intensified TV camera. Note that these detectors are not intrinsically species sensitive, so they can respond to both D–^{3}He and D–D fusion products (3 MeV protons and 1 MeV tritons) and also to escaping ^{3}He minority tail ions above $\approx$1 MeV. Therefore, a careful analysis of the experimental results is needed to determine the loss processes.

2. MEASUREMENTS OF MeV ION LOSS DURING ^{3}He MINORITY HEATING

Measurements of MeV ion loss were made during ^{3}He minority ICRH at 1.4 and 2.0 MA, both with and without simultaneous neutral beam injection (NBI), as shown in Table I. The data from the 90° detector are discussed in Sections 2.1–2.5, while the data from the 45° detector are discussed in Sections 2.6 and 2.7.

The ^{3}He minority concentrations were in the range of a few per cent in D majority plasmas, with a maximum ICRH power of 5.2 MW at 37 MHz, a resonant layer location within $\pm$5 cm of the plasma major radius of R_0 = 2.6 m, and a toroidal field B which varied from 4.6 to 4.9 T at R_0. The ICRH-only cases also had deuterium pellet fuelling just before the start of ICRH. The parallel deuterium NBI was with a power of up to 24 MW at 100 keV full energy.

Our approach here is to determine whether the observed loss is consistent with the first-orbit loss of

TABLE I. SHOT LIST FOR D–^{3}He

Shot range	I (MA)	ICRH (MW)	NBI (MW)
53220-53244	1.4	≤ 3.4	14–26
54264-54281	1.4	≤ 5.2	12–24
54308-54320	2.0	≤ 5.0	11–23
55505-55540	1.4	≤ 4.2	0
55451-55454	2.0	≤ 4.0	0

the D–^{3}He fusion products. Other possible MeV ion loss mechanisms are tail ion loss, such as observed previously with H minority heating [13, 14], and ICRH induced fusion product deconfinement, as discussed theoretically [15, 16].

The first-orbit loss characteristics of the D–^{3}He alpha particle should be very similar to those for the D–D fusion products, since the gyroradius of the 3.7 MeV D–^{3}He alpha particle is only about 10% larger than that of the 1 MeV triton or the 3 MeV proton. However, for the present thin scintillators, the 14.6 MeV proton produces about ten times less light per particle than the 3.7 MeV alpha (see Section 2.3), so it is nearly invisible in these experiments.

2.1. Time dependence of MeV ion loss during ICRH

Figure 1(a) shows the time dependence of the signal for total MeV ion loss from the 90° detector for a 1.4 MA, 19 MW NBI plasma with and without ^{3}He ICRH. The MeV ion signal increases by a factor of two to three during ICRH, even though the D–D fusion rate (proportional to the neutron rate) does not increase with ICRH, as shown in Fig. 2. Since the signal for NBI-only is due to first-orbit loss of D–D fusion products proportional to the neutron rate [17], the extra signal observed during ICRH is not due to the normal D–D first-orbit loss.

Figure 1(b) shows another 1.4 MA case with 4.6 MW of ICRH but without any NBI (#55540). After correction for camera gain, the lost MeV ion signal level in Fig. 1(b) is about 0.3 times that for the 19 MW NBI-only case in Fig. 1(a), even though the D–D reaction rate for ICRH-only is negligible ($\approx 3\times10^{13}$ n/s, Fig. 2). Thus, the MeV ion loss rate for ICRH-only is comparable to the ICRH induced loss during ICRH+NBI, consistent with a source due to D–^{3}He alphas. Note that the ICRH induced MeV ion loss starts and stops with the ICRH wave form, with a delay of ≈ 0.1 s, roughly as expected for tail ion formation.

2.2. Pitch angle and gyroradius distributions

Figure 3(a) compares the toroidal pitch angle (χ) distribution for the ICRH-only case of Fig. 1(b) with that for the NBI-only case of Fig. 1(a) (averaged over gyroradius ρ = 2–11 cm and ≈ 0.5 s). These two distributions are similar, and they are also similar to the distribution for the ICRH+NBI case in Fig. 1(a). Since the NBI-only χ distributions are consistent with first-orbit loss of D–D fusion products [17], the ICRH-only χ distribution is at least roughly consistent with the first-orbit loss of 3.7 MeV alphas with a similar gyroradius.

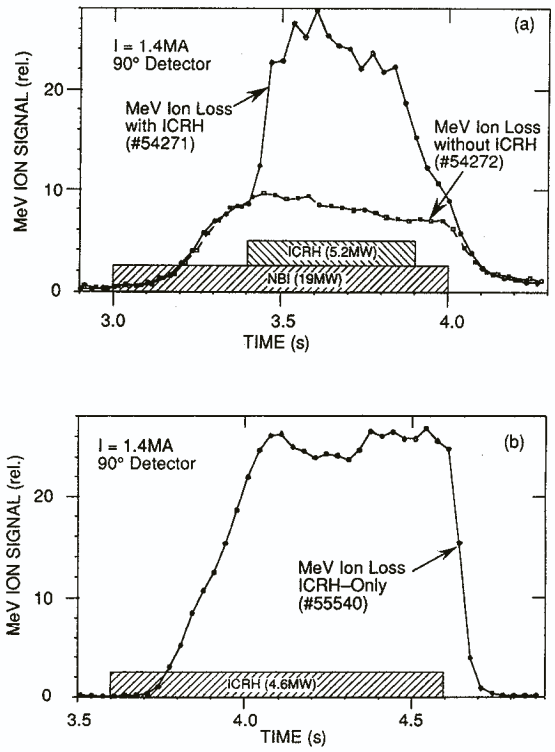

FIG. 1. MeV ion loss signals versus time to the 90° detector. (a) Increase (×2–3) in the MeV ion loss signal during 5.2 MW ICRH in a 19 MW NBI plasma. (b) MeV ion loss with 4.6 MW of ICRH alone (without NBI). These ICRH induced signals are interpreted as being due to first-orbit loss of the 3.7 MeV alpha particles from D–^{3}He reactions.

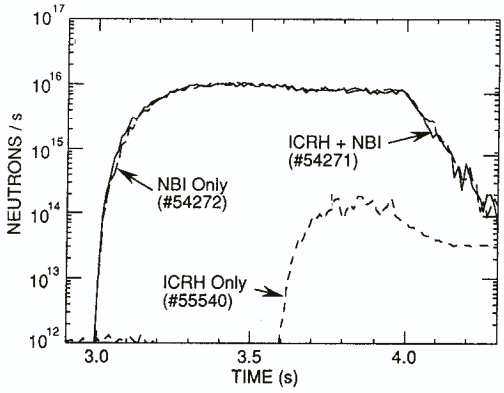

FIG. 2. 2.5 MeV neutron rates corresponding to the plasmas in Fig. 1. Note that the extra MeV ion loss during ICRH+NBI in Fig. 1(a) occurs without any increase in the D–D reaction rate.

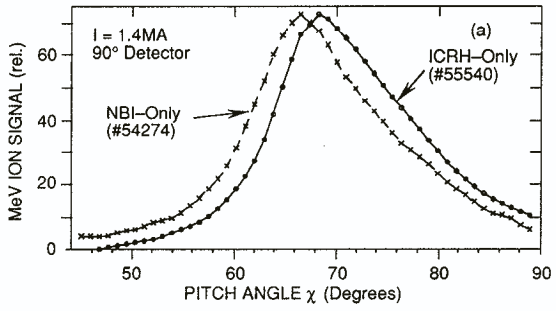

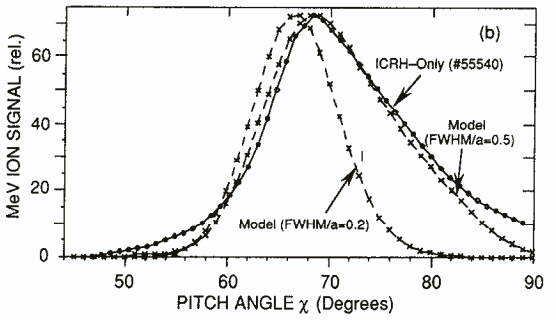

FIG. 3. MeV ion pitch angle distributions for the ICRH-only and NBI-only cases of Fig. 1. (a) The pitch angle distributions are similar, as expected, for first-orbit loss of D–D fusion products with NBI-only and of 3.7 MeV alphas with ICRH-only. (b) The ICRH-only distribution is consistent with first-orbit loss with a source profile width of FWHM/a = 0.5 (similar to the D–D fusion product profile).

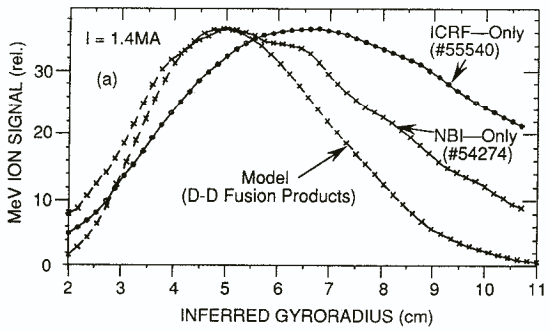

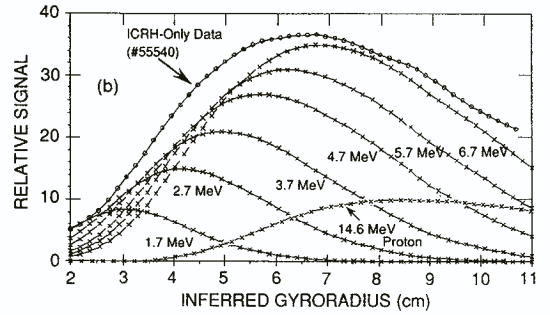

FIG. 4. MeV ion gyroradius distributions. (a) The gyroradius distribution for the ICRH-only case has a peak location at $\rho \approx 6.8$ cm, larger than the $\rho = 5.4$ cm expected for 3.7 MeV alphas (and larger than the 4.9 cm expected for the D–D fusion products). (b) The ICRH-only distribution is consistent with the loss of ≈5.7–6.7 MeV alphas. The shape of the expected 14.6 MeV proton distribution is also shown, although the magnitude of the proton contribution should be negligible.

This is shown explicitly in Fig. 3(b), which compares the ICRH-only distribution with that expected for first-orbit losses for 3.7 MeV alphas, including detector and optical broadening effects [17]. The calculated χ curve for an assumed D–^{3}He reaction rate profile of FWHM/a = 0.5 agrees well with the ICRH-only data. This reaction rate profile is similar to that for the D–D source (see Section 2.5).

Figure 4(a) shows the measured gyroradius (ρ) distributions for these NBI-only and ICRH-only plasmas (averaged over $\chi \approx 45$–$85°$ and ≈0.5 s). The ICRH-only case has a significantly larger loss at higher gyroradii than the NBI-only case, which is surprising since the expected gyroradius for first-orbit loss of 3.7 MeV alphas is only ≈10% larger than that for D–D fusion products, which are fairly well modelled by the expected D–D fusion product first-orbit loss at $\rho = 4.9$ cm.

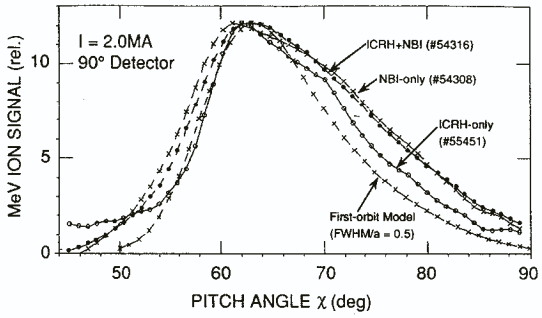

FIG. 5. Pitch angle distributions of the MeV ion loss during ICRH at 2.0 MA. The peak pitch angle shifts to lower values than those for the 1.4 MA case and is similar to that for an NBI-only plasma at the same NBI power, consistent with first-orbit loss of 3.7 MeV alphas in the ICRH-only case.

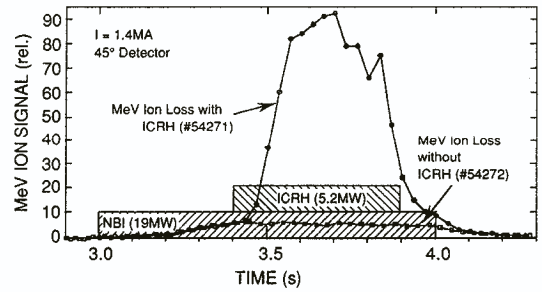

FIG. 6. MeV ion loss signal versus time from the 45° detector for a 1.4 MA plasma with ICRH+NBI. The MeV ion loss increases by a factor of >10 above the NBI-only level; this increase is much larger than the corresponding increase from the 90° detector shown in Fig. 1(a).

The ICRH-only gyroradius distribution is compared with the calculated shapes for various assumed alpha energies in Fig. 4(b), using the standard detector and optical resolutions [17], the appropriate foil attenuation factors and the estimated relative scintillator responses. The best fit to the ICRH-only distribution of Fig. 4(a) is obtained for an inferred alpha energy of 5.7–6.7 MeV instead of the expected energy of 3.7 MeV (see Section 3.1).

2.3. Response to 14.6 MeV protons

The total first-orbit loss rate for 14.6 MeV protons at 1.4–2.0 MA is up to ≈2 (5) times larger at 1.4 (2.0) MA than that for 3.7 MeV alphas, since the 14.6 MeV proton orbits can escape from the plasma centre, while the 3.7 MeV alpha orbits are lost only from r/a > 0.3. Thus the proton loss signal at twice the alpha gyroradius could potentially cause the shift to high ρ observed in the ICRH-only case of Fig. 4.

However, these detectors were not designed to measure 14.6 MeV protons, which have a range in ZnS of ≈1 mm, and should deposit <0.5 MeV in a 10 μm thick scintillator at ≈15–20° incidence [18]. The scintillator light emission from 14.6 MeV protons can be estimated from the measured 3 MeV proton response, which was ≈20% of that for a 3.5 MeV alpha [19. 20]. Since 3 MeV protons should deposit ≈1.0–1.5 MeV [18], the expected response for a 14.6 MeV proton is ≈0.05–0.1 times that of a 3.7 MeV alpha. The expected shape of the gyroradius distribution for 14.6 MeV protons has a broad peak near $\rho \approx$ 8–9 cm, as shown in Fig. 4(b).

However, the absence of a 14.6 MeV proton contribution to these signals can be seen in the gyroradius-averaged pitch angle distribution of Fig. 3, which does not have the expected proton first-orbit loss peak near $\chi \approx 78°$ [20]. Also, this gyroradius anomaly persists at low pitch angles (e.g. $\chi \approx 65°$ at 1.4 MA), at which the expected proton first-orbit loss rate is negligible. Therefore, 14.6 MeV protons do not cause the upward gyroradius shift seen in the ICRH-only measurements (see Section 3.1).

2.4. Plasma current dependence

At 2.0 MA, the time dependence and the gyroradius distribution of MeV ion loss were similar to those of

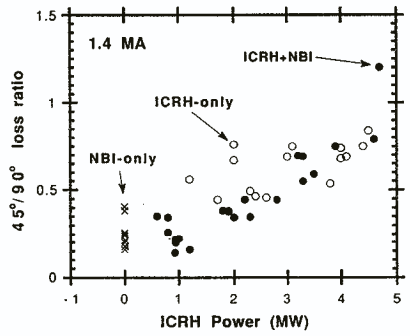

FIG. 7. Measured 45°/90° MeV ion loss ratio for various 1.4 MA plasmas. This ratio increases with ICRH power for both ICRH-only (1.0–4.5 MW) and ICRH+NBI (1.0–4.5 MW ICRH + 15–23 MW NBI), compared with the NBI-only cases (15–23 MW). This trend cannot easily be explained as first-orbit loss, implying an ICRH induced loss mechanism in the 45° detector. These data were digitized within pixels 26–32 and lines 9–15 (see Fig. 8).

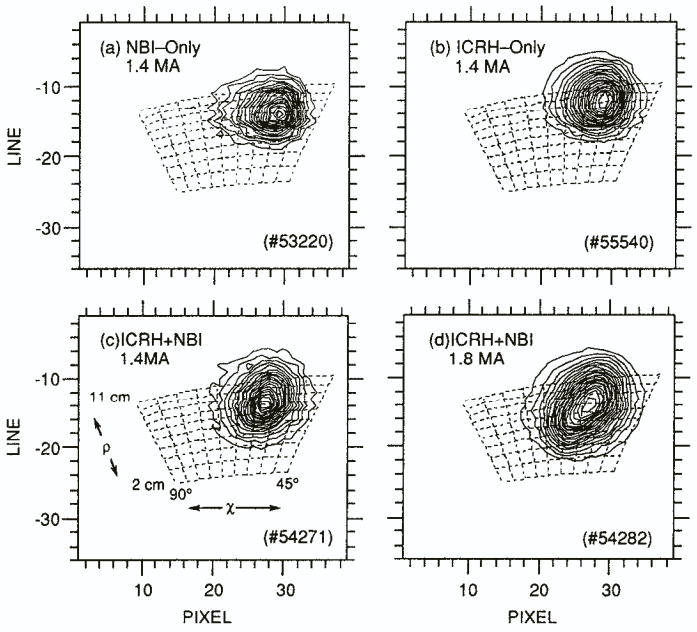

FIG. 8. 2-D (ρ, χ) patterns of the MeV ion signals in the 45° detector. The patterns for the NBI-only and ICRH-only cases in (a) and (b) are consistent with first-orbit loss of D–D fusion products and D–^{3}He alphas, respectively. The pattern with ICRH+NBI in (c) shows an unexpected distortion towards lower ρ and higher χ, associated with some ICRH induced loss mechanism. A larger distortion at 1.8 MA with ICRH+NBI is shown in (d).

1.4 MA plasmas mentioned in Section 2.3 (for further details see Ref. [21]). However, the pitch angle distribution in 2.0 MA plasmas had a peak near $\chi \approx 62°$ instead of $\chi \approx 68°$, as shown in Fig. 5 (together with a 2.0 MA NBI-only case). This shift agrees with the expected behaviour of first-orbit alpha loss at 2.0 MA, as shown by the model calculation and the NBI-only data in Fig. 5.

An increase in plasma current from 1.4 to 2.0 MA should also reduce the first-orbit loss fraction by a factor of two because of the decrease of the banana width. However, the relative alpha loss fraction versus current could not be determined since there was no independent measurement of the D–^{3}He reaction rates.

2.5. D–^{3}He radial source profile

The first orbit loss at each pitch angle corresponds to an integral over the source profile, but, for normally peaked sources, this integral is strongly weighted towards the radius closest to the plasma centre. Therefore, the radial source profile can in principle be inferred from the observed χ distribution (assuming only first-orbit loss).

Figure 3(b) shows good agreement between the observed χ distribution and a first-orbit alpha loss χ distribution calculated assuming a Gaussian source profile of FWHM/a = 0.5, but not a profile of FWHM/a = 0.2. This is confirmed by the similarity between the χ distributions during the ICRH+NBI and the NBI-only phases of the same plasma [21], implying that the D–^{3}He alpha source profile is nearly the same as the measured D–D source profile of FWHM/a = 0.55±0.15 [22]. The calculated D–^{3}He source profile is also close to this shape (Section 3.2). This profile shape can influence the interpretation of the observed loss to the 45° poloidal detector.

2.6. Results from the 45° poloidal detector

The total MeV ion signal versus time for the 45° detector, with and without ICRH, is shown in Fig. 6 for the same 19 MW NBI plasma as used in Fig. 1. During ICRH, the MeV ion loss signal at 45° increases by a factor of ≈10 above the NBI-only level, which is significantly larger than the increase by a factor of two to three above the NBI-only level seen in the 90° detector for the same plasma.

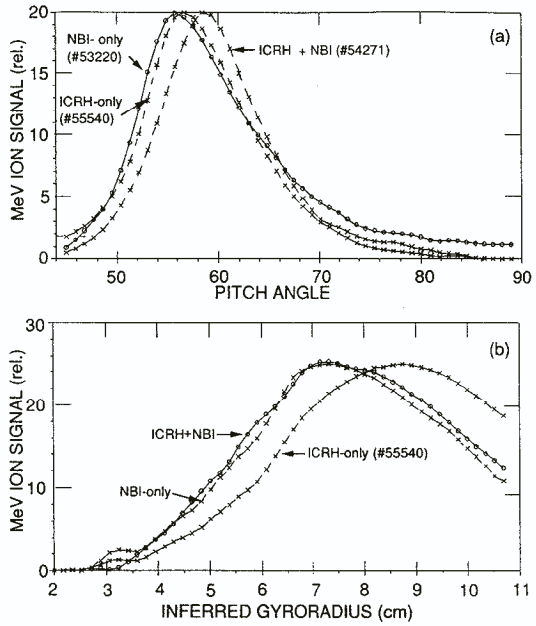

FIG. 9. Comparisons of (a) the pitch angle and (b) the gyroradius distributions for three of the patterns shown in Fig. 8. The ICRH+NBI case has a peak χ higher than that in either the NBI-only or ICRH-only cases, but a peak ρ similar to that for the NBI-only case. This anomaly suggests that the loss for ICRH+NBI is due to ICRH induced D–D fusion product loss.

Therefore, the poloidal distribution of the loss during ICRH is more heavily weighted towards 45° than the D–D fusion product first-orbit loss during NBI-only operation.

Figure 7 shows the relative 45°/90° MeV loss ratio versus ICRH power for a set of NBI-only, ICRH-only and ICRH+NBI plasmas, all at 1.4 MA. These signals were integrated over the peak (ρ, χ) region over most of the ICRH pulse (e.g. 3.5–3.8 s for NBI+ICRH) and corrected for the measured 45°/90° instrumental sensitivity ratio of 0.64 [19]. For the ICRH+NBI cases, the 45°/90° loss ratio increases with ICRH power from 0.3–0.6 for the NBI-only cases to 0.8–1.2 for the highest ICRH power. The 45°/90° loss ratio for ICRH-only is also larger than that for NBI-only, but it increases less rapidly with ICRH power. Note that the 45°/90° loss ratio expected for first-orbit loss of D–D or D–^{3}He fusion products is $\approx 0.4 \pm 0.1$, depending on the source profile (Section 3.3).

An interesting change in the shape of the (ρ, χ) loss pattern during ICRH+NBI can also be seen at 45°, as shown in Fig. 8. The NBI-only case is similar to the ICRH-only case, except for the somewhat larger gyroradius with ICRH. However, with ICRH+NBI there is an increased signal at an unusually low ρ and high χ which distorts the shape of the pattern significantly at 1.4 MA and even more at 1.8 MA.

This (ρ, χ) distortion is clarified by Fig. 9, which shows the χ distributions (averaged over ρ) and the ρ distributions (averaged over χ) for the 1.4 MA cases of Fig. 8. For NBI-only and ICRH-only, the χ distributions are similar, as expected for first-orbit loss of D–D and D–^{3}He fusion products, but for ICRH+NBI the loss peaks at a higher χ, corresponding to the loss of more deeply trapped ions. The ρ distribution with ICRH-only peaks at a higher gyroradius than that with NBI-only, similar to the 90° signals shown in Fig. 4, but the loss for ICRH+NBI has a ρ distribution similar to that of the NBI-only case, even though the latter is clearly dominated by ICRH induced loss (Fig. 6).

Part of the ICRH induced increase in the 45°/90° loss ratio shown in Fig. 7 might be explained by

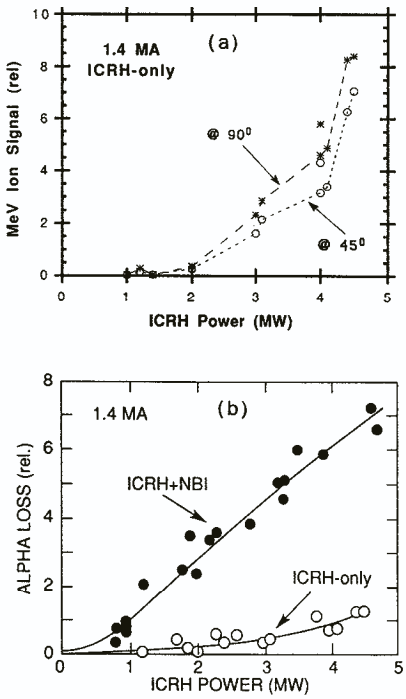

FIG. 10. Variation of the ICRH induced MeV ion loss signals with ICRH power. (a) The loss in both the 90° and 45° detectors increases proportionally to (ICRH power)^3 with ICRH-only. (b) ICRH induced loss in the 90° detector during ICRH+NBI. The ordinate is the inferred global D–^{3}He reaction rate (in units of 10^{15} reactions/s), assuming that these signals are due to first-orbit loss of alphas.

classical effects (Section 3.3). However, the distorted (χ, ρ) distribution for ICRH+NBI cannot be explained in this way, so it implies some ICRH wave induced deconfinement (Section 3.4). Note that no ICRH induced distortion was seen in the 90° detector.

2.7. MeV ion loss versus ICRH power

Figure 10(a) shows the increase in MeV ion loss for ICRH-only power at 1.4 MA. The loss at both 90° and 45° increased proportionally to (ICRH power)^3 over the range $\approx$1.0–4.5 MW, which is similar to the measured variation of the D–^{3}He reaction rate in PLT [23] and JET [24]. The shape of the (χ, ρ) distribution was constant over this power range, as expected for the first-orbit loss of D–^{3}He alphas in these cases with ICRH only.

Figure 10(b) shows the ICRH induced part of the loss at 90° versus ICRH power with 15–20 MW of simultaneous NBI. The ICRH induced loss for the ICRH+NBI cases was derived by subtracting out the expected contribution from D–D fusion products, as estimated from the pre-ICRH period with NBI-only [20]. At a given level of applied ICRH power, the ICRH induced loss is about 5–10 times larger with NBI (see Section 3.2).

The global D–^{3}He reaction rate can be inferred by comparing the ICRH induced loss during ICRH+NBI with the D–D fusion product loss during NBI-only, assuming that the 90° detector signals are due to first-orbit loss in both cases (i.e. assuming the same MeV ion loss fraction). After correcting for the 3.7 MeV alpha/(3 MeV proton + 1 MeV triton) ratio of $\approx$3 [18], the resulting global D–^{3}He reaction rate is given by the ordinate of Fig. 10(b) in units of 10^{15} reactions/s. This is comparable to the modelled reaction rates (Section 3.2).

3. THEORY AND MODELLING

The MeV ion loss measurements of Section 2 were consistent with first-orbit loss of D–^{3}He alpha particles, except for the unusually high gyroradius distribution noted in Section 2.2 and the increased 45°/90° loss ratio noted in Section 2.6. First attempts to understand these phenomena are described in this section.

3.1. Energy shift of D–^{3}He alpha loss

The most likely explanation for the higher than expected gyroradius of the observed D–^{3}He alpha particles (Figs 4 and 9) is the Doppler broadening ΔE expected owing to the high energy ^{3}He tail, which is $\Delta E \approx$ (1 MeV) $\sqrt{(T_{^3He}/200\ keV)}$ the temperature of $T_{^3He}$ [7, 25]. Therefore, creation of the inferred $\approx$5.7–6.7 MeV alphas would require a tail temperature of $T_{^3He} \approx$ 0.8 MeV, which is in fact close to the calculated ^{3}He tail temperature for these experiments (Section 3.2). Note that the pitch angle distribution expected for the first-orbit loss of 5.6 MeV alphas is only 2° higher than that for 3.7 MeV alphas, so it would still be consistent with the measured χ distribution of Fig. 3.

Although the alpha source spectrum should be broadened symmetrically about 3.7 MeV, the measured scintillator response is heavily weighted towards high alpha energies, for example by a factor of ten between 5.7 MeV and 1.7 MeV alphas (Fig. 4(b)). Also, higher energy alphas have a larger first-orbit loss, for example by a factor of three between 5.7 MeV and 1.7 MeV, further reducing the sensitivity to downshifted alphas. Therefore, it is most likely that the upshifted gyroradius distribution during ^{3}He ICRH experiments is due to alpha Doppler broadening; unfortunately, a detailed energy analysis is beyond the capability of the present detector.

Two other possible mechanisms for alpha energy shifts should be noted in passing. First, reactions between the ^{3}He tail and the NBI fast ions will also contribute to the Doppler width, but this rate should be proportional to the beam ion fraction (<10%). Second, ICRF heating of fusion product alpha particles might add to their energy up to $\approx$1 MeV (similar to the energy gain of ^{3}He), but the non-optimal resonant layer location for alphas makes this unlikely.

3.2. Calculation of the D–^{3}He reaction rate

The D–^{3}He reaction rate for a ^{3}He minority heated TFTR plasma was calculated using FPP/SPRUCE, a bounce averaged quasi-linear and Fokker–Planck code for comprehensive simulation of NBI and ICRH of tokamak plasmas [26, 27]. The modelled case had 5.2 MW of ICRH power and 23 MW NBI at 2.0 MA (#54320). The calculated D–^{3}He source profile had a FWHM/a $\approx$ 0.5 and a total source rate of $\approx 1.6\times10^{16}$ D–^{3}He reactions/s (equivalent to 45 kW of D–^{3}He fusion power). The average energy of the ^{3}He tail near the plasma centre was $\approx 1.2\pm0.2$ MeV (i.e. a 0.8 MeV tail temperature). The predicted D–^{3}He rate was somewhat sensitive to the assumed ^{3}He concentration (which was based on the measured density rise during the ^{3}He gas puff, but which assumed 100% recycling

and ignored any ^{3}He residual from previous plasmas). Doubling the ^{3}He concentration from 1.25% to 2.5% causes the predicted D–^{3}He rate to increase only by 50%, since the increase in the number of ^{3}He ions is partially offset by the drop in their average energy.

Analysis of the 90° MeV ion loss data from the closest available plasma with 3.7 MW ICRH at 2 MA (i.e. #54316) gives a global D–^{3}He reaction rate of $\approx 0.9\times10^{16}$ alphas/s, as inferred from the ratio of the escaping alpha flux during ICRH to the escaping D–D fusion product flux during NBI (Section 2.7). If the D–^{3}He reaction rate for ICRH+NBI increases linearly with ICRH power, as in Fig. 10(b), then the inferred reaction rate for 5.2 MW ICRH power would be $\approx 1.3\times10^{16}$ reactions/s, i.e. consistent with the calculation. The model inferred source profile of FWHM/a = 0.5 is also consistent with the measured pitch angle distributions at 2 MA shown in Fig. 5. Therefore, the MeV ion loss measured in the 90° detector at 2 MA is approximately consistent with the expected first-orbit loss of D–^{3}He alpha particles (with an uncertainty of a factor of two to three).

A interesting feature of the data of Fig. 10(b) is that the D–^{3}He reaction rate is about five times larger with simultaneous 15–20 MW NBI than without NBI. This can be explained by the higher central electron temperature with NBI, implying less ion drag and therefore a higher ^{3}He tail temperature and a higher D–^{3}He reaction rate. For example, a typical case with ICRH-only (#55540) has $T_e(0) \approx 5.5$ keV at $n_e(0) = 5\times10^{13}$ cm^{-3}, while for ICRH+NBI (#54271), $T_e(0) \approx 8$ keV at $n_e(0) = 4\times10^{13}$ cm^{-3}; thus, the high energy ion drag $\alpha T_e^{3/2}/n_e$ is lower by a factor of approximately two with NBI, implying a higher tail energy by this factor (at fixed ICRH power) and so a higher D–^{3}He reaction rate by roughly a factor of four. The large uncertainty in the relative ^{3}He concentration between these two cases makes a more quantitative comparison difficult at this stage.

3.3. Source profile effects on the expected 45°/90° ratio

The increase in the 45°/90° loss ratio by a factor of two to three for ICRH+NBI compared to NBI-only (Fig. 7) suggested an ICRH induced MeV ion loss at 45°. However, another possible cause of this increase is the variability of the first-orbit loss rate versus the shape of the source profile, since detectors at different poloidal angles sample orbits from different spatial regions.

The 45°/90° first-orbit loss ratio for D–^{3}He alphas was calculated, using the standard orbit code, as a function of the assumed Gaussian source profile width. This ratio was 0.4 at FWHM/a = 0.5, but, with a narrower source profile, it increased up to ≈ 1.2 at FWHM/a = 0.2. However, such a narrow source profile is inconsistent with the measured pitch angle distribution at 90°, which implied FWHM/a $\approx$ 0.5 and not FWHM/a = 0.2 (see Figs 3 and 5); it is also inconsistent with the reaction rate calculation, which predicted FWHM/a $\approx$ 0.5 (Section 3.2).

However, the D–^{3}He source profile should have some poloidal asymmetry because ICRH causes the ^{3}He banana tips to lie near the resonance layer (R $\approx$ 2.63 m). A modelling study of this effect was made by assuming that the D–^{3}He source was confined to a vertical band at a variable R, with a vertical FWHM/a = 0.5 or 1.0 and a horizontal Gaussian FWHM/a = 0.1. The calculated 45°/90° first-orbit loss ratios for a 1.4 MA plasma varied from 0.2 to 0.6 for the range of assumed asymmetries [21], with the largest ratio being ≈ 0.6 for a profile peaked at R $\approx$ 2.9 m with a vertical FWHM/a = 0.5. The tentative conclusion from this modelling is that the result of Fig. 7 with asymmetry ratios of up to 1.2 cannot be explained solely by first-orbit loss.

3.4. ICRH induced MeV ion loss

Evidence was presented in Section 2 that the poloidal asymmetry of the MeV ion loss increased with ICRH power (Fig. 7) and that the (ρ, χ) loss patterns at 45° were distorted towards higher χ and lower ρ with ICRH+NBI (Figs 8 and 9). Since these effects could not be readily explained by either first-orbit loss or toroidal field ripple loss (see Section 3.3), it is interesting to consider whether they could be due to either direct ICRH minority tail ion loss or ICRH induced deconfinement of D–D or D–^{3}He fusion products.

These two possible mechanisms have different implications for future D–T tokamaks with ICRH. If the observed loss at 45° was due to ^{3}He tail ions, it would be from ions with $\approx(3\text{–}5)T_{^3He}$ in a tail with $T_{^3He} \approx 1$ MeV and $n_{^3He}/n_e \approx 0.01$, and such a loss would not increase significantly with a switch to D–T operation. However, if this loss were due to ICRH induced deconfinement of fusion products, it would imply a much larger fractional loss of the relatively small confined fusion product population ($< 10^{-4}$ n_e for these experiments), and so this loss could increase by

a factor of ≈ 100 during D–T operation, assuming a similar effect with D–T alphas.

Another way of describing this difference is in terms of power loss. In the absence of ICRH, the fusion product power loss is ≈ 1 kW, assuming $\approx 10\%$ first-orbit loss with a source rate of $\approx 2\times10^{16}$ D–D fusions/s (Fig. 6). Since the MeV ion loss increases by a factor of ten in the 45° detector during ICRH, the total MeV ion loss observed during ICRH is < 10 kW. This is still much smaller than the ≈ 3 MW of ICRH power going into the ICRH tail in these experiments. Thus, the anomalous loss during ICRH can be explained by either a very small fractional loss of the ICRH tail ($\approx 1\%$) or a large fractional loss of the confined fusion products.

Unfortunately, it is not possible to directly distinguish between tail ion loss and fusion product deconfinement in the present experiment, since the detectors are not sensitive to species differences (for example between ^{3}He, ^{4}He and ^{3}H), but only to gyroradii, and since the expected gyroradii of tail ions and fusion products can be similar. Indirect distinctions between these mechanisms are also difficult, since the population of D–^{3}He alphas is proportional to the population of the high energy ^{3}He ion tail.

However, some progress can be made from theoretical considerations. One possible mechanism for ICRH induced fast ion loss is due to the radial step which trapped fast ions can experience when their banana tip passes through the resonant layer [15]. Note that the first harmonic resonance (in the $k_\parallel = 0$ limit) occurs for ^{3}He tail ions with banana tips near R = 2.6 m and also for D–^{3}He alpha particles with banana tips at R = 2.0 m, whereas the second harmonic resonance occurs for D–D tritons with banana tips at R = 2.6 m (Doppler broadening can also be large for these energetic ions). Previous calculations for JET suggested that such an ICRH induced diffusion could reduce the stored energy in the ^{3}He ion tail by up to 20% [16] because of radial movement of tail ions out from the hot core.

A theoretical estimate of the ICRH wave induced radial diffusion coefficient D for tail ions which gain all their energy from (symmetrically launched) ICRH waves is [15]: $D \approx k_\phi^2\rho^2\rho_\theta^2/\tau_w$, where k_ϕ is the toroidal wavenumber of ICRH, ρ and ρ_θ are the toroidal and poloidal tail ion gyroradii, and $\tau_w = \tau_s/2$ is the collisional energy equilibration time between the tail ions and the background plasma. The average radial distance over which a particle will diffuse in a time τ_w is thus $\Delta r \approx (2D\tau_w)^{1/2} \approx 1.4\, k_\phi\rho\rho_\theta$. For the TFTR case of Section 3.2, with ICRH+NBI, $k_\phi \approx 20/R$, $\rho \approx 3$ cm (for a ^{3}He ion with ≈ 1.2 MeV) and $\rho_\theta = (R/r)q\rho \approx 30$ cm, so that ICRH would transport the tail ions a distance of only ≈ 10 cm. Since this is much smaller than the plasma minor radius of 95 cm, it appears to be too small to explain the increased loss at 45°.

The above formula for ICRH induced diffusion is not directly applicable to fusion products, since their energy does not come solely from ICRH. Other equations from Ref. [15] have been used to estimate that D–^{3}He alphas would also be transported ≈ 10 cm by ICRH in a time τ_w, but that D–D tritons would be transported a much smaller distance. Thus it also appears that ICRH induced diffusion of fusion products cannot explain the increased loss at 45°.

Fast ions might also be lost if ICRH would significantly increase their banana widths. However, the amount of energy δW that an ion of energy W absorbs from ICRH during one pass through the resonance layer is very small, i.e. $\delta W/W \approx \tau_b/2\tau_w \approx 10^{-5}$, where τ_b is the bounce time for a 1 MeV ^{3}He ion. Therefore, this small step size per bounce $\delta\rho_b$ would cause the loss to be highly localized just below the midplane within a poloidal angle $\theta_{loss} \approx a\cos([1 + \delta\rho_b/\rho_b)]^{-2}) \approx 2(\delta\rho_b/\rho_b)^{1/2} < 1°$ below the outer midplane. It is difficult to see how any small-step transport process such as that discussed above could cause a loss 45° below the midplane, unless it combines with a large-step loss mechanism near the plasma edge. This tendency for loss to occur near the midplane also explains (at least qualitatively) why no ICRH induced loss is observed at 90° below the midplane.

3.5. Toroidal field ripple loss

Stochastic toroidal field ripple diffusion is a process which could lead to a large enough step size near the plasma edge to explain the observed loss at 45°. The maximum radial step size is $\delta r/\rho_b \approx \mathrm{sqrt}(\pi Nq)\,(R\delta/r)$, where N is the number of field coils and δ is the ripple strength [19]. For a barely confined 1.2 MeV ^{3}He ion with its banana tip at r = 80 cm and $\theta = 90°$, the ripple is $\delta \approx 3\times10^{-3}$ and the radial step size is $\delta r/\rho_b \approx 0.15$. If two ripple induced steps would add coherently, the poloidal loss angle would be $\theta_{loss} > 50°$, more than enough to be visible in the 45° detector. Although the toroidal field ripple decreases towards the interior, at r/a = 0.5 the ripple could still cause diffusion over an average distance of $\Delta r \approx 30$ cm. Since the loss of only $\approx 1\%$ of the ^{3}He ions could explain

the observed signals at 45°, it appears that toroidal field ripple assisted loss is a possible explanation.

Note that stochastic toroidal field ripple loss calculations show that D–D fusion product loss should mainly be localized within ≈30° of the outer midplane and be small compared with first-orbit loss for the 45° detector [19]. However, ripple loss of ≈1% of trapped tail ions at 45° is plausible, given the statistics of the poloidal distributions in that calculation.

3.6. Large angle collisions

Another possible candidate for explaining the anomalous losses during ICRH is classical large angle collisions. The rate of 90° scattering of fast ions in a single collision is smaller than the usual small angle scattering rate by a factor of $\ln\Lambda \approx 20$. In such a collision, a 3 MeV ^{3}He ion with its banana tip at r = a/4 could be carried out to r ≈ a/2. The power transferred by such collisions is roughly

$$P_{LAC} \approx \nu_{LAC} FW \approx (1/\ln\Lambda)\nu_{ti}\tau_w FP_{RF}$$

where ν_{LAC} is the large angle scattering rate, ν_{ti} is the usual pitch angle scattering rate, W is the stored energy in the ^{3}He tail, and F is the fraction of the energy in ions of >3 MeV (which have a sufficiently large banana width to be lost in one event), where F ≈ 0.15 for a Maxwellian with T = 800 keV, and $P_{RF} \approx 3.6$ MW. Using the relation

$$\nu_{ti}\tau_w = Z_{eff}/[2A < Z_i^2/A_i > (1 + E^{3/2}/E_{crit}^{3/2})]$$

where $E_{crit} \approx 140$ keV for ^{3}He, A = 3, $\langle Z_i^2/A_i \rangle = 0.5$ and $Z_{eff} = 3$, we find that $P_{LAC} \approx 0.3$ kW for E > 3 MeV. This is considerably less than the estimated 10 kW loss due to ICRH (Section 3.2), suggesting that this mechanism is not the dominant cause of the observed loss with ICRH. However, a more detailed calculation should be done to include, for example, the influence of the somewhat more probable moderate angle collisions on the tail ion loss.

4. SUMMARY AND CONCLUSIONS

We have described measurements and modelling of MeV ion loss observed during ^{3}He minority ICRH in TFTR. At 90° below the midplane, the pitch angle (χ) distribution, the gyroradius (ρ) distribution and the absolute flux of lost MeV ions were consistent with the expected first-orbit loss of fusion product alpha particles, given the calculated D–^{3}He source profile, Doppler shift and reaction rate. This behaviour is similar to the D–D fusion product loss, although the absence of a direct measurement of the D–^{3}He reaction rate made the interpretation here more difficult.

However, the detector 45° below the outer midplane showed evidence for an ICRH induced MeV ion loss mechanism for ICRH+NBI, which at the highest ICRH power increased the 45°/90° loss ratio by up to a factor of approximately two to three above the expected first-orbit loss and also caused an added loss at unexpectedly low ρ and high χ. These effects are most likely due to the loss of a small fraction of the ^{3}He minority tail, although ICRH induced deconfinement of fusion products cannot be completely ruled out, given the lack of species selectivity of the present detectors.

This point could be further clarified by varying the majority and minority species during both ICRH-only and ICRH+NBI. For example, replacement of the D majority by ^{4}He could (without NBI) separate the D–^{3}He alpha production from the ^{3}He tail loss, and variation of the D–D reaction rate due to NBI at a fixed ICRH power might also separate the possible wave induced D–D fusion product loss from the direct tail ion loss. Detection of ions nearer the outer midplane would also help clarify the poloidal distribution of the ICRH induced loss, which would be needed to better estimate the total ICRH induced loss fraction.

The ICRH induced MeV ion loss described here could affect the interpretation of future D–T alpha particle experiments with NBI+ICRH, such as those planned for TFTR and JET, since it may be difficult to distinguish between ICRH induced loss and alpha instability induced loss. Also, since the tolerable MeV ion loss rate in large D–T machines such as ITER is only a few per cent, because of possible localized first wall damage [28], the poloidal distribution and plasma current scaling of this ICRH induced loss should be better understood before designing the ITER first wall.

ACKNOWLEDGEMENTS

We thank E. Fredrickson, J. Hosea, L. Johnson, D. Mikkelsen, D.K. Owens, J.Y. Park, J.D. Strachan, J. Stevens and K.M. Young for contributions to this paper, and T.H. Stix for suggesting the large angle scattering mechanism for tail ion losses.

REFERENCES

[1] JET Team, JACQUINOT, J., BHATNAGAR, V.P., BUREŠ, M., et al., in Plasma Physics and Controlled Nucler Fusion Research 1990 (Proc. 13th Int. Conf. Washington, DC, 1990), Vol. 1, IAEA, Vienna (1991) 679.

[2] HOSEA, J.C, BEER, M., BELL, M.G., et al., ibid., p. 669.
[3] CHRIEN, R.E., STRACHAN, J.D., Phys. Fluids **26** (1983) 1953.
[4] HEIDBRINK, W.W., Nucl. Fusion **24** (1984) 636.
[5] LOVBERG, J.A., HEIDBRINK, W.W., STRACHAN, J.D., ZAVERYAEV, V.S., Phys. Fluids **B 1** (1989) 874.
[6] HEIDBRINK, W.W., CHRIEN, R.E., STRACHAN, J.D., Nucl. Fusion **23** (1983) 917.
[7] STRACHAN, J.D., Nucl. Fusion **29** (1989) 163.
[8] MARTIN, G., JARVIS, O.N., KÄLLNE, J., MERLO, V., SADLER, G., VAN BELLE, P., Phys. Scr. **T 116** (1987) 171.
[9] MURPHY, T.J., STRACHAN, J.D., Nucl. Fusion **25** (1985) 383.
[10] SADLER, G.J., CONROY, S.W., JARVIS, O.W., VAN BELLE, P., ADAMS, J.M., HONE, M.A., Fusion Technol. **18** (1990) 556.
[11] MEDLEY, S.S. (PPPL), personal communication, 1991.
[12] ZWEBEN, S.J., BOIVIN, R.L., DIESSO, M., et al., Nucl. Fusion **30** (1990) 1551.
[13] MANOS, D.M., STANGEBY, P.C., BUDNY, R.V., COHEN, S.A., KILPATRICK, S., SATAKE, T., J. Nucl. Mater. **129** (1984) 319.
[14] HOSEA, J.C., PHILLIPS, C.K., STEVENS, J.E., et al., in Theory of Fusion Plasmas (Proc. Joint Varenna–Lausanne Int. Workshop Varenna, 1990), Editrice Compositori, Bologna (1990) 223.
[15] CHEN, L., VACLAVIK, J., HAMMETT, G.W., Nucl. Fusion **28** (1988) 389.
[16] CORE, W.G.F., Nucl. Fusion **29** (1989) 1101.
[17] ZWEBEN, S.J., BOIVIN, R.L., CHANG, C.-S., HAMMETT, G.W., MYNICK, H.E., Nucl. Fusion **31** (1991) 2219.
[18] ZIEGLER, J.F., Helium Stopping Powers and Ranges in all Elemental Materials, Vol. 4, Pergamon Press, New York (1977).
[19] BOIVIN, R., Measurements of Charged Fusion Product Diffusion in TFTR, Rep. PPPL-2797, Princeton Plasma Physics Laboratory, Princeton, NJ (1991).
[20] TUSZEWSKI, M., ZWEBEN, S.J., Calibration of Scintillator Detectors for MeV Charged Fusion Products, Rep. LA-UR92-903, Los Alamos National Laboratory (1991); to be published in Rev. Sci. Instrum.
[21] ZWEBEN, S.J., HAMMETT, G.H., BOIVIN, R., PHILLIPS, C.K., WILSON, R., MeV Ion Loss During ^{3}He Minority Heating in TFTR, Rep. PPPL-2812, Princeton Plasma Physics Laboratory, Princeton, NJ (1992).
[22] JOHNSON, L. (PPPL), personal communication, 1991.
[23] CHRIEN, R.E., STRACHAN, J.D., Phys. Fluids **23** (1983) 917.
[24] JACQUINOT, J., SADLER, G., and the JET team, D–^{3}He Fusion in the JET Tokamak — Recent Experimental Results, Rep. JET-P(91)07, JET Joint Undertaking, Abingdon, Oxfordshire (1991).
[25] SADLER, G., JET Team, "Fast particles in JET plasmas", in Alpha Particles (Proc. IAEA Tech. Comm. Mtg Göteborg, 1991), to be published.
[26] SMITHE, D.N., PHILLIPS, C.K., HAMMETT, G.W., COLESTOCK, P.L., in Applications of Radio-Frequency Power to Plasmas (Proc. 8th Top. Conf. Irvine, CA, 1989), American Institute of Physics, New York (1989) 338.
[27] HAMMETT, G.W., DORLAND, W., KAITA, R., MEDLEY, S.S., SMITHE, D.N., COLESTOCK, P.L., ibid., p. 258.
[28] POST, D., BORRASS, K., CALLEN, J.D., et al., ITER Physics, ITER Documentation Series No. 21, IAEA, Vienna (1991).

(Manuscript received 28 November 1991
Final manuscript received 1 June 1992)